RSC Advances

PAPER

View Article Online
View Journal | View Issue

Cite this: *RSC Adv.*, 2018, **8**, 38391

Surface modified $Li_4Ti_5O_{12}$ by paper templated approach for enhanced interfacial Li^+ charge transfer in Li-ion batteries†

Ujjwala V. Kawade,[a] Manish S. Jayswal,[a] Anuradha A. Ambalkar,[a] Sunil R. Kadam,[b] Rajendra P. Panmand,[a] Jalinder D. Ambekar,[a] Milind V. Kulkarni*[a] and Bharat B. Kale*[a]

The $Li_4Ti_5O_{12}$ (LTO) and lithium silicate (LS) surface modified LTO have been demonstrated by a unique paper templated method. Comparative study of structural characterization with electrochemical analysis was demonstrated for pristine and modified $Li_4Ti_5O_{12}$. Structural and morphological study shows the existence of the cubic spinel structure with highly crystalline 250–300 nm size particles. The LS modified LTO shows the deposition of 10–20 nm sized LS nanoparticles on cuboidal LTO. Further, X-ray photoelectron spectroscopy (XPS) confirms the existence of Li_2SiO_3 (LS) in the modified LTO. The electrochemical performance was investigated by cyclic voltammetry (CV), electrochemical impedance spectroscopy (EIS) and galvanostatic charge–discharge. The modified LTO with 2% LS (LTS2) exhibited excellent rate capability compare to pristine LTO *i.e.* 182 mA h g^{-1} specific capacity at a current rate, 50 mA g^{-1} with remarkable cycling stability up to 1100 cycles at a current rate of 800 mA g^{-1}. The lithium ion full cell of modified LTO with LS as an anode and $LiCoO_2$ as a cathode exhibited a remarkably reversible specific capacity *i.e.* 110 mA h g^{-1}. Both electronic and ionic conductivities of pristine LTO are observed to be enhanced by incorporation of appropriate amount of LS in LTO due to a larger surface contact at the interface of electrode and electrolyte. More significantly, the versatile paper templated synthesis approach of modified LTO with LS provides densely packed highly crystalline particles. Additionally, it exhibits lower Warburg coefficient and higher Li ion diffusion coefficient which in turn accelerate the interfacial charge transfer process, which is responsible for enhanced stable electrochemical performance. The detailed mechanism is expressed and elaborated for better understanding of enhanced electrochemical performance due to the surface modification.

Received 25th September 2018
Accepted 6th November 2018

DOI: 10.1039/c8ra07953f

rsc.li/rsc-advances

1. Introduction

Graphite has been widely used as a common anode material for lithium ion batteries (LIBs) but it possesses some demerits such as, some graphite material peel off from the current collector during lithiation/delithiation of Li-ions. At high rate Li-ion diffusion in graphite is low and the charge/discharge potential around 0.1 V (*vs.* Li/Li^+) hence Li dendrites formation take place in graphite which reduces the electrochemical performance and also generate safety issues. These combined limitations restrict the application of graphite in LIBs.[1–3] Lithiation and delithiation ability of lithium titanium oxide was first reported by Murphy *et al.* in 1983.[4] Recently many reports have signified enormous attention on $Li_4Ti_5O_{12}$ (LTO) as an excellent anode material for LIBs. LTO is considered to be the most suitable anode material in LIBs for energy storage due to some excellent electrochemical properties, such as a stable and high voltage plateau of 1.5 V *vs.* Li/Li^+, high safety, high rate capability, long cycling performance and ease of synthesis. Lithiated LTO's higher potential *versus* lithium makes it more stable and safer than lithiated graphite, due to a reduction in the driving force for lithium dendrite formation. The LTO has excellent reversibility and long stable cyclability in LIBs due to negligible volume expansion during intercalation/deintercalation of Li ions.[5–10] Especially LTO has a "zero-strain" structure during charge and discharge processes in the lithium ion battery applications.[10–12] The LTO has cubic crystal structure with $Fd\bar{3}m$ space group, where O_2^- is located at 32e sites, 3/4 of Li^+ is located at tetrahedral 8a sites and the rest of Li^+ with Ti^{4+} is located at octahedral 16d sites with a unit cell parameter of 0.836 nm. The reaction mechanism with lithiation and delithiation during electrochemical reaction has been reported.[12,13]

[a]*Centre for Materials for Electronics Technology (C-MET), Ministry of Electronics and Information Technology (MeitY), Panchavati, Pune 411008, India. E-mail: bbkale@cmet.gov.in; milind@cmet.gov.in*

[b]*Department of Physics, Savitribai Phule Pune University, Ganeshkhind, Pune 411007, India*

† Electronic supplementary information (ESI) available. See DOI: 10.1039/c8ra07953f

At counter electrode,

$$\mathrm{Li} \rightleftharpoons x\mathrm{Li} + x\mathrm{e}^- \quad (1)$$

Intercalation at LTO working electrode,

$$3\mathrm{Li}^+ + 3\mathrm{e}^- + \mathrm{Li_4Ti_5O_{12}} \rightleftharpoons \mathrm{Li_7Ti_5O_{12}} \quad (2)$$

Even at zero-strain, during reaction LTO has some intrinsic kinetics drawbacks because of its low electrical conductivity (*ca.* 10^{-8} to 10^{-13} S cm^{-1})[14,15] and low lithium diffusion coefficient (*ca.* 10^{-9} to 10^{-16} cm^2 s^{-1}),[16] which limits its rate capacity. Efforts have been devoted to enhance the specific capacity by improving the electronic conductivity as well as ionic conductivity *via* surface modifications within LTO. Diverse modifications in LTO were carried out by doping of metal and non-metals, coating with carbonaceous materials (carbon, graphene, CNT), size reduction up to nano-regime and composite strategies.[14,17–30] The fundamental thought behind these modifications is that to increase anion adsorption, electronic conductivity, and decrease the polarization and ionic energy barrier. This modification to enhance interfacial charge transfer involves both lithium ions and electrons which ultimately enhance the electrochemical performance. However, these improvements are marginal to satisfy the high rate capability demanded by electric vehicles.

To avoid the gassing behaviour and to reduce adverse interfacial side reactions of active materials, chemically inert substances were used for surface modifications on electrode.[15,31] But due to the lower electronic and ionic conductivities of the coating materials, the electrochemical performance of LTO is still an inadequate. Therefore, choosing proper chemically inert coating substances to improve conductivity is necessary to enhance the electrochemical performance of the LTO. Most of the researchers have reported surface modification of cathode and anode using solid electrolytes which displayed outstanding lithium ion conduction and effectively improved electrochemical performance.[31–38] Many researchers have synthesized LTO using different synthesis approach to address the effect of surface modification to enhance the electrochemical performance. Also, efforts have been taken to find more effective surface modifier to enhanced capacity with stability. Recently, $Li_4Ti_5O_{12}$ surface was modified with TiO_2, SiO_2, TiO_2–SiO_2 and Li_2SiO_3 *etc. via* solvothermal/hydrothermal followed by annealing, sol–gel method, cellulose-assisted combustion technique and emulsion system.[16,19,23,27] Among these as a surface modifying agent, Li_2SiO_3 has recently attracted as a coating for anode materials due to its high ionic conductivity. It acts as a Li^+-ion conductor to enhance the ionic conductivity for anode as well as cathode materials for LIBs.[15,19,39] Li_2SiO_3 acts as a most excellent surface modifier because it gives stability to the electrode materials and avoids the side reactions and giving more Li^+ ions during lithiation/delithiation processes which accelerates the capacity.[39]

The voltage of LTO batteries lower than graphite batteries. But cubic spinel LTO anode has a three orders of magnitude lower risk of short circuiting than commercial graphite anodes which is confirmed by short circuit abuse tests (ISCAT).[40,41] Therefore, as a potential anode for LIBs, the LTO electrode has been used efficiently in batteries. Jansen *et al.*[42] reported a full cell of LTO with a $LiCoO_2$ as a cathode material with its cycling performance up to 117 000. Then, the compatibility of LTO anode with layered $LiCoO_2$ and its hybrids materials have been studied to ensure the electrochemical performance at around 2.5 V. Additionally, the LTO anode with a layered type $LiCoO_2$ cathode in full cell exhibits higher energy density than its hybrids materials such as $LiNi_{1/3}Co_{1/3}$, $Mn_{1/3}O_2$ and $LiMn_2O_4$ cathodes.

Thus, based on the our earlier report,[43] we have demonstrated pristine $Li_4Ti_5O_{12}$ and surface modified nanocomposites of $Li_4Ti_5O_{12}$ with lithium silicate (Li_2SiO_3) by the whatman paper mediated template method as an anode material for lithium-ion batteries. $Li_4Ti_5O_{12}$, modification with Li_2SiO_3 has been carried out by *in situ* synthesis method for the first time. The comparative study of structural characterization with electrochemical analysis was demonstrated for pristine and modified $Li_4Ti_5O_{12}$. The modified anode composite exhibits significant enhancement in the specific capacity and rate capability for high-performance lithium-ion batteries. After evaluation of the electrochemical performances of all LTO electrodes in half-cell assembly, its full cells has been fabricated and electrochemical performance has been demonstrated.

2. Experimental methods

2.1 Material preparation

All the reagents were analytical pristine grade and used without further purification. $Li_4Ti_5O_{12}$ anode materials were synthesized by a versatile template method according to our previous work.[43] Stoichiometric amounts of lithium acetate ($LiAc\cdot 2H_2O$, 99.0%, Aldrich) and tetraethyl orthotitanate ($Ti(OC_2H_5)_4$, 99%, Aldrich) were dissolved in anhydrous ethanol. Nitric acid was added to avoid the precipitation of tetraethyl orthotitanate. After dissolved completely, the stoichiometric amount of tetraethyl orthosilicate ($Si(OC_2H_5)_4$, Aldrich) was added drop-wise in the above solution under continuous stirring. The mixture was magnetically stirred for 30 min to obtain homogeneous mixing. The above solution was impregnated in the ash less Whatman filter paper and dried at room temperature. The papers were calcined at 300 °C for 3 h in air. After calcination, the powders were ground again to fine powders and followed by sintering at 900 °C for 4 h. Heating rate was kept constant at 5 °C min^{-1} for all processes during the synthesis. For fabricating surface modified $Li_4Ti_5O_{12}$, the $Si(OC_2H_5)_4$ solution was added *i.e.* silicate accounting for 1, 2 and 3 wt% in the mixture, and the products are assigned to LTS1, LTS2 and LTS3 in order. To get the pristine $Li_4Ti_5O_{12}$ anode material the same synthesis process without addition of $Si(OC_2H_5)_4$ was used and the product is named as PLTO.

2.2 Material characterization

The crystal structures of the $Li_4Ti_5O_{12}$ anode nanostructures were examined with powder X-ray diffraction technique (XRD,

Bruker Advanced D8) using Cu Kα radiation source. The morphological and micro-structural analysis of as-synthesized $Li_4Ti_5O_{12}$ nanostructures were investigated with field emission scanning electron microscopy (FESEM, Hitachi, S-4800) and field emission transmission electron microscopy (FETEM by JEOL; JEM-2200FS). The surface chemical composition was studied with X-ray photoelectron spectroscopy (XPS, Thermo Fisher Scientific Co., Theta Probe). Room temperature micro Raman scattering was performed using a HR 800-Raman Spectroscopy, Horiba JobinYvon, France, with an excitation at 532 nm.

2.3 Electrochemical measurements

To perform electrochemical measurements 2032 type coin cells were used. The active material, conducting carbon and polyvinylidene fluoride (PVDF) binder were mixed in a weight ratio of 80 : 10 : 10 in *N*-methyl-2-pyrrolidone (NMP) as a solvent. The prepared slurry was casted onto copper current collector with help of a doctor-blade and kept for drying in vacuum oven for 12 h, at 120 °C, which was further used as a working electrode. After drying under ambient condition, round discs of 16 mm diameter were punched and further dried under vacuum at 120 °C for 12 h. The 2032 coin type half-cells were assembled in an argon-filled glove box, using metallic lithium foil (75 μm in thickness) as the counter and reference electrode, quartz filter paper as the separator, 1 M $LiPF_6$ in ethylene carbonate (EC) : dimethyl carbonate (DMC) (1 : 1 in volume) (BASF) as the electrolyte, and the round discs as working electrodes. Lithium cobalt oxide (LCO, MTI Corp.) slurry were prepared by mixing the active material, conducting carbon and Polyvinylidene fluoride (PVDF) binder were mixed in a weight ratio of 80 : 10 : 10 in *N*-methyl-2-pyrrolidone (NMP) as a solvent. The prepared slurry was casted onto aluminum current collector and kept for drying in vacuum oven for 12 h, at 120 °C, which further used as a cathode electrode. The 2032 type full cells were prepared by using LCO/LTO (LTS2) electrode. Their electrochemical measurements (galvanostatic charge–discharge tests) were carried out on MTI make battery analyzer (*vs.* Li/Li^+) at room temperature. Cyclic voltammetry behaviour of the half cells was tested on the Autolab potentiostat/galvanostatic instruments (Metrohm Autolab) between 1 V to 2.5 V with scan rate of 0.2 mV s^{-1}. Electrochemical impedance spectroscopy was performed using amplitude of 5 mV with a frequency range from 0.1 Hz to 1 MHz.

3. Results and discussion

The detailed phase formation mechanism for PLTO and modified LTO composite nanomaterials, *via* versatile paper template method schematically illustrated in Fig. 1. The ethanolic solution lithium acetate, tetraethyl orthotitanate and tetraethyl orthosilicate was absorbed in the Whatman paper and dried at 80 °C and further calcined at 300 °C. During calcination, $Ti(OH)_4$ and $Si(OH)_4$ slowly condensed into amorphous TiO_2 and SiO_2. Then this powder was grinded in pestle mortar

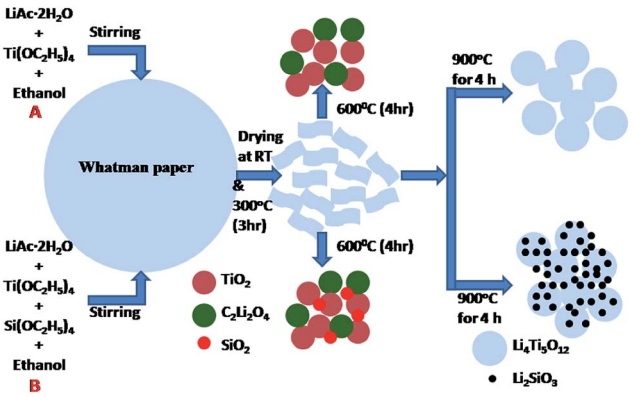

Fig. 1 Schematic diagram of the formation mechanism process of the LTO and surface modified LTO.

for homogenization of intermediates formed and further used for next steps.

$$4C_2H_3LiO_2\cdot 2H_2O + 5Ti(OC_2H_5) \rightarrow 5TiO_2 + 2C_2Li_2O_2 \quad (3)$$

$$5TiO_2 + 2C_2Li_2O_4 \rightarrow Li_4Ti_5O_{12} + CO_2 \quad (4)$$

$$4C_2H_3LiO_2\cdot 2H_2O + Si(OC_2H_5)_4 + 5Ti(OC_2H_5)_4 \rightarrow 5TiO_2 + 2C_2Li_2O_4 + SiO_2 \quad (5)$$

$$5TiO_2 + 3C_2Li_2O_4 + SiO_2 \rightarrow Li_4Ti_5O_{12} + Li_2SiO_3 + nCO_2 \quad (6)$$

When calcined at 600 °C for 4 h, titanium oxide (TiO_2) and lithium oxalate ($C_2Li_2O_4$) phase formation take place as per reaction 3. Further as per reaction 4, the TiO_2 react with $C_2Li_2O_4$ and form the $Li_4Ti_5O_{12}$ at 800 °C (Fig. 1A). Fig. S1 in ESI† shows the X-ray diffraction patterns of samples calcined at 600, 700 and 800 °C. However, at 800 °C, the LTO crystal grows at [400] direction instead of [111] plane. For LIBs, $Li_4Ti_5O_{12}$ spinel structure is essential with the unit cell parameter 0.836 nm for a "zero strain effect". Thus, final sintering of intermediates at 900 °C for 4 h has been performed to accelerate the growth of [111] plane for cubic spinel structure. For surface modification, along with LTO precursor's tetraethyl orthosilicate was also added. Hence, along with TiO_2 and $C_2Li_2O_4$, formation of SiO_2 is also taking place at 600 °C. Since, the concentration of SiO_2 is very less and due to amorphous state, XRD peaks are not detected. When the sintering was carried out for surface modified samples, SiO_2 reacts with $C_2Li_2O_4$ and formation of Li_2SiO_3 take place along with LTO at 900 °C as per the eqn (6) (Fig. 1B).

Fig. 2 shows the X-ray diffraction patterns of synthesized $Li_4Ti_5O_{12}$ (PLTO) and silicate modified $Li_4Ti_5O_{12}$ (LTS1, LTS2, LTS3) with varying $Si(OC_2H_5)_4$ concentration. The pristine $Li_4Ti_5O_{12}$ shows formation of highly crystalline cubic spinel phase (Fig. 2, PLTO). The silicate modified $Li_4Ti_5O_{12}$ prepared with varying the $Si(OC_2H_5)_4$ concentrations also shows formation of cubic spinel structure. For all samples, there are sharp diffraction peaks at 2θ values of 18.20, 35.59, 43.27, 47.41, 57.19, 62.62, 66.03, 74.4, 75.12 and 79.22 which can be assigned to the

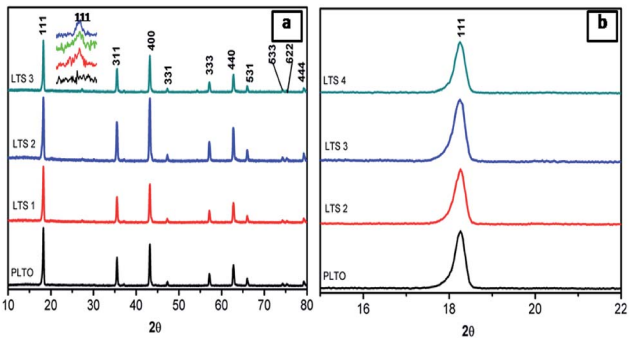

Fig. 2 XRD patterns of pristine $Li_4Ti_5O_{12}$ (PLTO) and silicate modified $Li_4Ti_5O_{12}$ (LTS1, LTS2 and LTS3) samples.

[111], [311], [400], [331], [333], [440], [531], [533], [622] and [444] planes of face centered cubic spinel $Li_4Ti_5O_{12}$ phase (JCPDS card no. 049-0207). Fig. 2b shows the magnified [111] peak of LTO reveals a slight peak shift to a lower theta. As discussed, silicate precursor was mixed with the precursor of LTO and sintered at 900 °C for 4 h which leads not only to form interface bond, but also confer solid diffusion near the interface between LTO and silicate compound (Li_2SiO_3). This is due to the large octahedral (1.9854 nm) and tetrahedral (1.9963 nm) interstices in LTO.[44] Generally, due to the smaller radius of Si^{4+} (0.04 nm) than Ti^{4+} (0.06 nm) and Li^+ (0.076 nm), the substitution of Si^{4+} for Ti^{4+} or Li^+ exhibit lattice shrinkage.[16] Thus the lower 2θ shift of diffraction peaks after coating with LS is very likely to be induced the interstitial sites of LTO as similar to F-doped LTO.[28] The diffraction peaks of Li_2SiO_3 are detected in silicate modified $Li_4Ti_5O_{12}$. In the silicate modified sample, peak at 27.01 corresponds to [111] plane of the Li_2SiO_3 phase shown in inset of Fig. 1a (JCPDS card no. 00-029-0829) which is absent in case of PLTO. In XRD, absence of impurity peaks other than LS suggesting the high phase purity of the nanocomposite.

The morphological study of PLTO and the surface modified LTO with Li_2SiO_3 by FESEM are depicted in Fig. 3a–d. It is observed that both LTO samples possess a well-crystalline structure, suggesting retaining in the morphology of LTO. As shown in Fig. 3a and b several particles are interconnected to form a chain like structure with dense network having diameter in the range of 200–500 nm. When silicon was introduced, the diameter of particles was reduced (Fig. 3b), The LTS2 (2% silicate) indicates the increased the particles linkage and network (Fig. 3c and d). This interconnected network which may be responsible in shortening the transport path of lithium ions and electrons. Overall, with varying silicon concentration, the morphology does not show any significant difference but the formation of denser network is observed (Fig. S2 in ESI†).

Accordingly, further investigated the surface microstructure of the PLTO and surface modified LTO (2%) using field emission transmission electron microscope (FETEM) has been performed. The low and high resolution FETEM images of PLTO (Fig. 4) and LTS2 (Fig. 5) nanostructures, along with selected area electron diffraction pattern (Fig. 4d and 5c) shows highly crystalline interconnected nanoparticle network. The SAED image shows many bright diffraction spots indicating that the both samples have good crystalline characteristic. The pristine PLTO sample depicts formation of spherical shaped 100–200 nm size particles aligned each other. Fig. 5b shows a uniform distribution of Li_2SiO_3 nanoparticles having size in the range of 20–30 nm on the surface of LTO. The FETEM of PLTO and LTS2 samples depicts the inter-planar spacing of 0.248 and 0.24 nm corresponds to [101] and [111] plane exhibit spinel structure.

The silicate modified $Li_4Ti_5O_{12}$ (LTS2) was further analyzed using EDS (Fig. 5e–h) for elemental mapping images which demonstrate that all Li_2SiO_3 nanoparticles homogeneously coated on LTO particles. LTO and LS particles are interconnected and forms interface bond, as well as the solid diffusion near the interface between LTO and LS due to

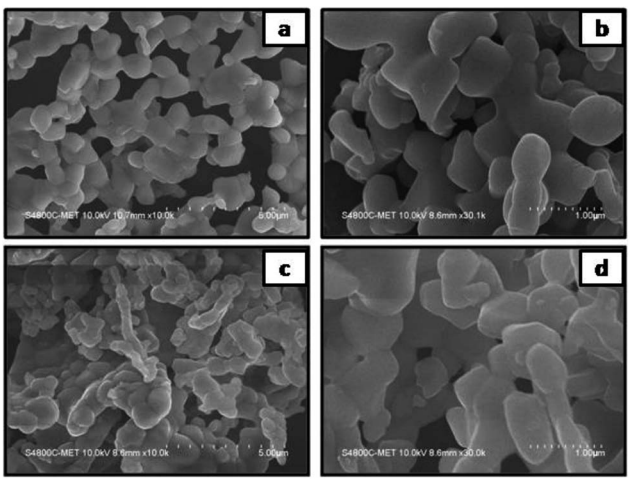

Fig. 3 FESEM images of (a and b) pristine $Li_4Ti_5O_{12}$ (PLTO) and (c and d) the silicate modified $Li_4Ti_5O_{12}$ (LTS2) at low and high magnifications.

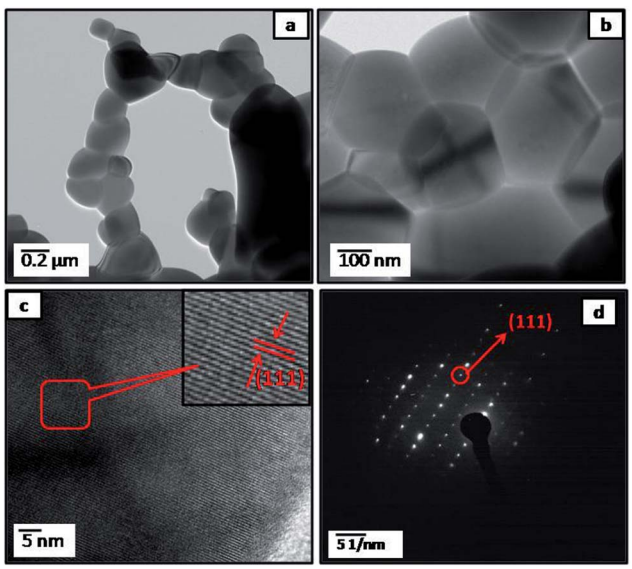

Fig. 4 FETEM images of pristine $Li_4Ti_5O_{12}$ (PLTO) (a and b) at different magnifications; (c) FETEM of the individual $Li_4Ti_5O_{12}$ at high resolution; (d) corresponding SAED patterns.

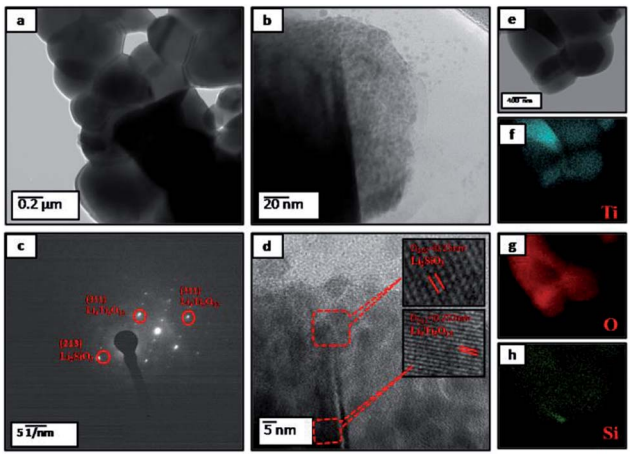

Fig. 5 FETEM images of pristine silicate modified $Li_4Ti_5O_{12}$ (LTS2) (a and b) at different magnifications; (c) corresponding SAED patterns; (d) HRTEM of the individual $Li_4Ti_5O_{12}$ (e) STEM image of $Li_4Ti_5O_{12}$ and EDS mappings: colour map of (f) Ti, (g) O and (h) Si.

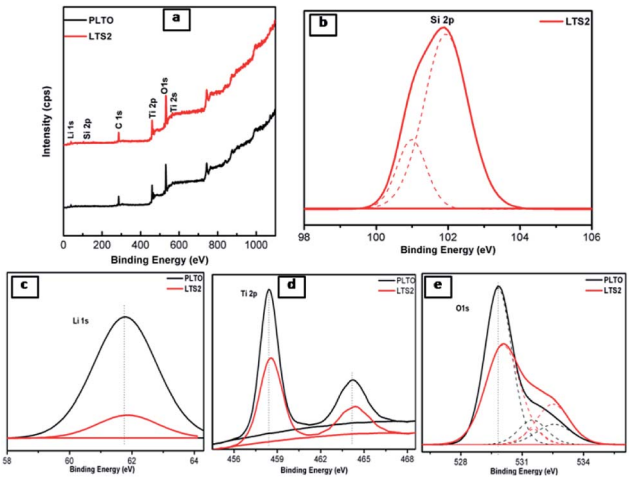

Fig. 7 (a) XPS survey scan PLTO and silicate modified $Li_4Ti_5O_{12}$ (LTS2: 2%) and XPS spectra of (b) Li, (c) Ti, (d) Si, (e) O.

sintering. The silicate nanoparticles prevent the stacking of LTO nanoparticles as well as buffer the expansion volume of Li–Si during cycling.

Further, Raman of pristine LTO and surface modified LTO shows the comparison of their shifting to longer wavelength due to surface modification (Fig. 6a). Raman spectrum shows typical bands located at 673 and 751 cm^{-1}, which correspond to the vibrations of Ti–O bonds in TiO_6 octahedra, the two bands located at 348 and 425 cm^{-1} are ascribed to the stretching vibrations of Li–O bonds.[45] It can be clearly seen that prominent peak centered at 234 cm^{-1} is due to the bending vibrations of O–Ti–O and O–Li–O bonds.[46] In the spectra, for pristine LTO and surface modified LTO, all the above mentioned Raman bands are observed for the spinel $Li_4Ti_5O_{12}$ too.

In case of silicate modified sample bands of LTO exhibit a slight shift to the higher wavelength with broadening (Fig. 6b) which suggests that the surface coating on LTO simultaneously changes the inner chemical environment of LTO, giving rise to the weakening of the cation–oxygen bonds and the increment in lattice constant.[47] A further observation reveals that the peak intensity of Raman spectra decreases gradually in samples from LTS1–LTS3 composite with the increasing silicate content, implying the Si^{4+} content enhanced degree of disorder. Therefore, the Raman result reveals that the successful incorporation of Si^{4+} into the interstitial sites of LTO to impair the Li–O and Ti–O bonding.[15]

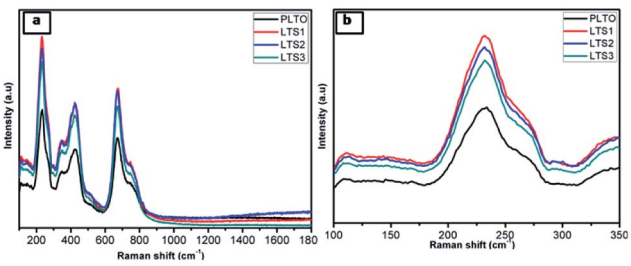

Fig. 6 Raman spectra of (a) all $Li_4Ti_5O_{12}$ (PLTO, LTS1, LTS2 and LTS3) samples (b) compares the magnified Raman signature.

To investigate the surface elements, their chemical state and binding natures, X-ray photoelectron spectroscopy (XPS) measurements were conducted. Fig. 7 shows the survey spectrum of LTS1 and LTS3 samples which depicts the existence of Si, Li, Ti, and O elements related to LTO. Along with these elements, LTS2 shows Si corresponds to silicon components. The Si 2p peak could be deconvoluted into two peaks (Fig. 7b). Out of these, one peak located at 101.9 eV due to Li_2SiO_3 while the other for SiO_2 (100.9 eV) from the Si–O bond in SiO_2. This result confirms the existence of Li_2SiO_3 and SiO_2 within the LTO phase. It is worth noting that the diffraction peaks of SiO_2 in XRD cannot be detected in silicate modified $Li_4Ti_5O_{12}$ which might be due to the low content and amorphous state of SiO_2.[48] Fig. 7c shows Li 1s peak occurs at 61.7 and 61.8 eV for PLTO and LTS2 sample respectively. The Ti 2p presented Ti $2p_{1/2}$ peak centered at 464.40 eV and Ti $2p_{3/2}$ around 458.56 eV which depicts that the oxidation state of the Ti cations is four (IV) in PLTO and LTS2 as shown in Fig. 7d.[48–50] Fig. 7e, shows the O 1s peak at 530 eV and 531.5 eV observed are related to TiO_2, while the peak at 532.5 eV observed is associated with oxygen bonded with silicon. In addition, in every peak, the binding energies of modified LTO are shifted to longer wavelength with lowering in intensity than that pristine LTO due to the existence of Li_2SiO_3 and SiO_2.

4. Electrochemical study

The electrochemical performance of individual LTO samples was identically investigated using a coin-type half cell. Cyclic voltammograms (CVs) curves of PLTO, LTS1, LTS3 and LTS4 are shown in Fig. 8a. The anodic peaks at about 1.65 V (*vs.* Li/Li^+) and the cathodic peaks at around 1.49 V (*vs.* Li/Li^+) are correspond to the processes of Li de-intercalation and intercalation within the spinel $Li_4Ti_5O_{12}$. The result clearly demonstrates that there is a pair of similar reversible redox peaks for pure LTO and

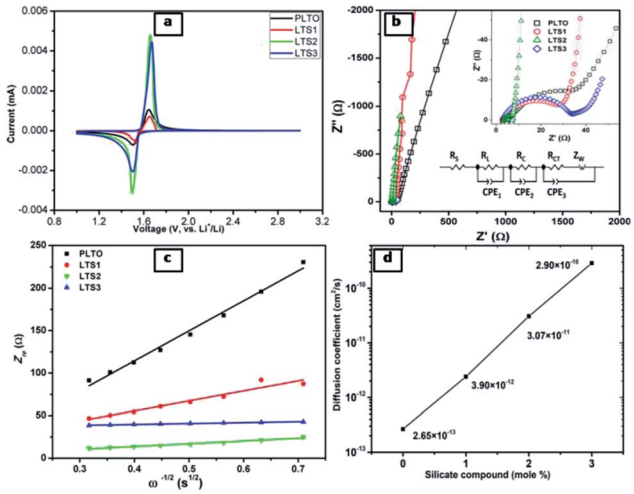

Fig. 8 (a) Cyclic voltammetry curves of all LTO samples (PLTO, LTS1, LTS2 and LTS3) electrode at a scan rate of 0.2 mV s^{-1}. (b) Electrochemical impedance spectrum and inset is enlarged spectra in the high-medium frequency region and equivalent circuit model. (c) The relationship between Z_{re} and $\omega^{-1/2}$. (d) The relationship between Li^+ diffusion coefficient with mole% of silicate compound.

modified LTO, suggesting that Li_2SiO_3 do not change the electrochemical reaction process of LTO. But the intensity of cathodic and anodic peaks of the LTS2 sample are higher and sharper compared to the PLTO. The peaks reflect the better electrode kinetic which enhances the charge–discharge capacity of modified $Li_4Ti_5O_{12}$ (LTS2).

Fig. 8b shows the AC impedance spectra of the all LTO electrodes, which are measured at the identical conditions. The impedance spectra are simulated with the given equivalent circuit and the results are presented in Table 1 for resistance (R) values. In this circuit R_S, R_L, R_C and R_{CT} are electrolyte resistance, resistance of LS coating, connection resistance of active nanoparticles and charge transfer resistance, respectively. The charge transfer resistance of LTS2 (7.63 Ω) is less than that of the pristine PLTO (35.43 Ω), most likely because of the availability of Li ions which increases charge transfer process at the electrode/electrolyte interface. The exchange current density (i_0) behaviour of all LTO samples are evaluated by the eqn (7)[48] and values are presented in Table 1.

$$i_0 = \frac{RT}{nFR_{CT}} \quad (7)$$

These results reveal that LTS2 sample has higher exchange current density (3.38 mA cm^{-2}) than PLTO sample (0.72 mA cm^{-2}) which confirms that silicate coating on LTO effectively increases the Li^+ ion diffusion which controls the interfacial resistance between particles during the electrochemical reactions. During the charge–discharge cycling, electrolyte soaks into the silicate compounds to form solid electrolyte which enhances the ionic conductivity of LTO particles. In this case, Li_2SiO_3 and amorphous SiO_2 on the LTO surface provide larger contact area at the interface of electrode and electrolyte which in turn may accelerate Li^+ ion diffusion. Additionally to investigate the effect of surface modification on LTO in terms of Li^+ ion diffusion calculated from the relationship between Z_{re} and $\omega^{-1/2}$ in the low frequency region using the following equations.[15,51]

$$Z_{re} = R_S + R_{CT} + \sigma_w \omega^{-\frac{1}{2}} \quad (8)$$

$$D = \frac{R^2T^2}{2A^2n^4F^4C^2\sigma_w{}^2} \quad (9)$$

where ω is angular frequency in the low frequency region, σ_w represents the Warburg impedance coefficient, D is Li^+ diffusion coefficient, R is gas constant, T is absolute temperature, A is area of electrode surface n is the number of the electrons per molecule participating in the electronic transfer reaction, F is Faraday constant and C is the molar concentration of Li^+.[52] Fig. 8c shows the correlation between Z_{re} and $\omega^{-1/2}$ for PLTO, LTS1, LTS2 and LTS3 samples in the low frequency region and the slope of the fitted line is the Warburg coefficient σ. The Warburg coefficients are 353.41, 117.74, 32.87 and 10.70 Ω, and diffusion coefficients of lithium ion are calculated to be 9.41×10^{-17}, 8.48×10^{-16}, 1.09×10^{-14} and 1.03×10^{-13} cm^2 s^{-1} for PLTO, LTS1, LTS2 and LTS3, respectively. It clearly shows that with increasing the concentration of Li_2SiO_3, the Warburg coefficient decreases however Li ion diffusion coefficient increases. As compared to pristine LTO the modified LTO, the silicate compounds shows enhance the lithium-ion diffusion and decrease the charge transfer resistance, which is favourable for the electrochemical performance of the electrodes. The ionic conductivity is increased due to the incorporation of Li_2SiO_3 while SiO_2 effectively reduce the electrochemical polarization within LTO. It is expected to improve the electrochemical activity of modified LTO, which is similar to that of other reported surface-modified electrode materials for lithium-ion batteries.[53,54] Fig. 8d clearly shows a linear relationship between diffusion coefficients with concentration of silicate compound within the modified LTO. But with 3% silicate incorporation, ionic conductivity of LTO enhances but electronic conductivity decreases, dramatically due to shielding in migration and transport of electron.

The discharge–charge behaviours of the individual composite electrodes are performed by galvanostat. The electrochemical performance of the LTO and modified LTO is shown in Fig. 9. The rate potential of the LTO and surface modified LTO are tested at the current densities from 50 to 1600 mA g^{-1} (Fig. 9a), respectively. Accordingly, the reversible discharge capacities obtained at various current densities are summarized in Table 2.

From the Table 2, it is observed that the reversible capacities of coated LTS2 are higher than those of pristine LTO (PLTO) at

Table 1 Fitted parameters of equivalent circuit

Sample	R_S (Ω)	R_L (Ω)	R_C (Ω)	R_{CT} (Ω)	i_0 (mA cm^{-2})
PLTO	4.64	41.75	12 551	35.43	0.72
LTS1	2.769	27.22	17 320	28.60	0.90
LTS2	3.338	4.17	3317	7.63	3.38
LTS3	1.871	26.45	901.4	33.7	0.76

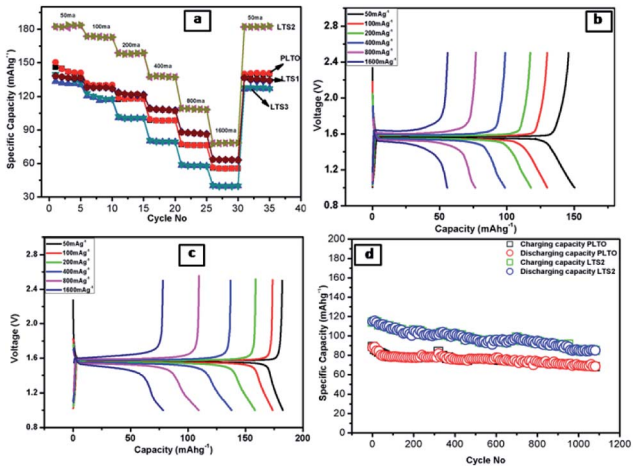

Fig. 9 Electrochemical properties of: (a) the rate performance of all samples at different current densities (b and c) the initial discharge–charge profiles at different current rate (a-PLTO and b-LTS2) and (d) cycling performance of PLTO and LTS2 between 1 and 2.5 V at the current rate of 800 mA g^{-1}.

the respective current densities. For pristine LTO the initial discharge/charge capacities are 150/146 mA h g^{-1} and for modified LTO (LTS2) 182/183 mA h g^{-1}. The reversible capacity for PLTO and LTS2 are 141 and 183 mA h g^{-1} retains after 5th cycles at 50 mA g^{-1}, respectively. More significantly, it reveals better Li-intercalation maintained after cycling at different current densities. The initial coulombic efficiencies are observed to be 95.68, 97.33, 99.45 and 99.8% for PLTO, LTS1, LTS2 and LTS3, respectively. All the samples shows higher coulombic efficiency for first cycle reveals less SEI formation and better stability of the electrode due to interconnected particle network. At the maximum discharging rate *i.e.* 1600 mA g^{-1} C (~10C), the LTS2 delivers a reversible capacity of 77 mA h g^{-1} which is higher than that of PLTO (56 mA h g^{-1}). Moreover, recovery rate of LTS2 is observed to be ~100% while for PLTO is 93% when the current density reverts to 50 from 1600 mA g^{-1}. Fig. 9a depicts that as the current rate revert back from high to low, the specific capacity observed almost similar to initial capacity. This recovery clearly demonstrates that the stability of the LTO anode material which retained even after high current rate to lower during discharge/charge processes.

The modified LTO electrodes with 1% silicate, initially shows lower capacity than pristine LTO but having good rate capability at high current. Sample LTS2 exhibited higher capacity with better rate capability because of the interface bonding between LTO and LS which improved Li^+ transport due the sintering. However, the LTS3 sample shows capacity decrease with the increasing amount of silicate (3%).

The better electrochemical performances for LTS2 confirm the favourable effect of optimum LS coating. Fig. 9b and c show the galvanostatic discharge/charge performance plateau at different current rates for PLTO and modified LTS2, respectively. A small amount of ionic conductor Li_2SiO_3, gives stability to the active material, additionally provides three-dimensional Li^+ channels which favour the diffusion of Li^+ ions, during discharging/charging process. By expanding the voltage plateau at around 1.3 V *vs.* Li/Li^+ which ultimately enhances the capacity. The LTS3 demonstrate further suppressed electron migration and results in reduced cycling performance with a reversible capacity of 139 mA h g^{-1} than the LTS2 (182 mA h g^{-1}) at 50 mA g^{-1} current rate. Due to excess LS there is increases ionic conductivity but reduction in electronic conductivity which is responsible for getting lower capacity for LTS3. To evaluate the polarization effects during galvanostatic charge/discharge, the potential interval (ΔV) between the initial discharge/charge plateaus is calculated for lower and higher current rates (50 and 1600 mA g^{-1}) shown in Fig. 10. The potential interval is smaller for LTS2 compared to pristine PLTO. From Table 1, it is observed that the connection resistance RC among active particles is decreasing with increasing silicate concentration which is correlated with the ΔV values of respective samples. This suggests that, during cycling lithium silicate helps in reducing the polarization of Li^+ ions. The cycling performance of PLTO and LTS2 samples was tested at the current rate of 800 mA g^{-1} for 1100 cycles between 1–2.5 V. The discharge capacities for PLTO and LTS2 samples were observed to be 67 and 88 mA h g^{-1} after 1100 cycles with 100%

Table 2 Discharge capacities at various current densities

Cycle no.	Current rate (mA g^{-1})	Specific capacity (mA h g^{-1})			
		PLTO	LTS1	LTS2	LTS3
1	50	150	138	182	139
6	100	131	128	174	123
11	200	118	123	158	102
16	400	99	109	138	81
21	800	78	88	109	59
26	1600	56	64	77	40
31	50	140	137	182	128

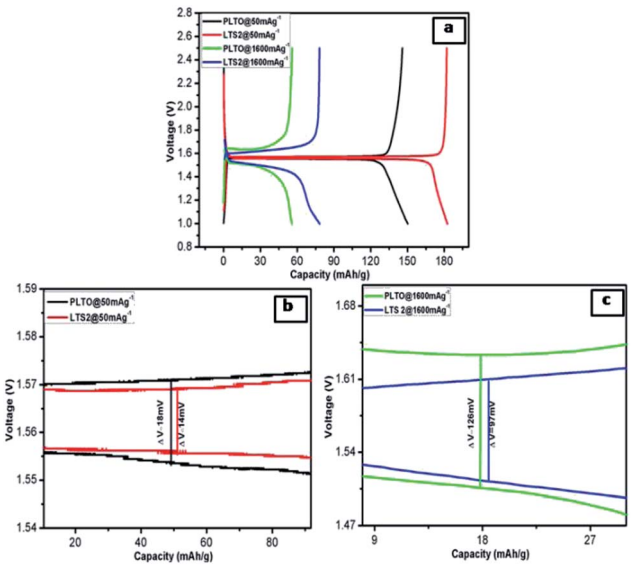

Fig. 10 (a) Comparison of the initial discharge–charge profiles of PLTO and LTS2 at 50 and 1600 mA g^{-1} and (b) 50 mA g^{-1} (c) 1600 mA g^{-1}.

coulombic efficiency, respectively. It is noteworthy that at high current rate *i.e.* 800 mA g^{-1}, the LTS2 electrode exhibits long-term cycling stability (88 mA h g^{-1} after 1100 cycles) with marginal capacity fading due to the insignificant volume change of LTO during cycling.

The pristine and modified $Li_4Ti_5O_{12}$ synthesized *via* template method shows the efficient rate capability and cycling stability at 800 mA g^{-1}, which serve as potential anode materials for high-performance LIBs. This improvement in performance is ascribed to the, interconnecting network of nanoparticles as well as surface modification in LTO having zero-strain property. Therefore, during cycling LTO has negligible volume change, which is an advantage for good cyclability and rate capability. In the surface modified system, Li_2SiO_3 nanoparticles increases ionic conductivity of Li ions and giving more Li^+ ions during lithiation/delithiation processes and reduces the polarization which enhances the capacity. Surface modification exhibit creation in vacancies in LTO which inhibit the recombination of charge carrier. It is responsible for enhancement in the electrochemical properties of LTO. Additionally, Li_2SiO_3 nanoparticles with SiO_2 form shielding layer on LTO against the electrolyte which suppresses the side reactions at the interfaces, which is beneficial to reduce the gassing behaviour and provide stability to the electrode materials.[13] But some researchers emphasized more on the electrochemical activity than the Li^+ diffusion at the high rate discharge processes. From the lithium ion diffusion coefficient Li_2SiO_3 exhibits excellent ionic conductivity, but its higher concentration decreases the specific capacity of LTO electrodes. At 3% silicate compound within LTO further suppressed electron migration and results in lower electronic conductivity during electrochemical reaction resulting in reduced cycling performance. Hence, surface modification of LTO with appropriate amount of silicate compound exhibits moderate ionic conductivity, good electrical conductivity with lower polarization which gives good reversible capacity and rate capability.

After electrochemical performances study of half-cells, the full cells with $LiCoO_2$ as a cathode and LTS2 as anode were fabricated. Fig. 11a shows charge–discharge curve of the full cell and Fig. 11b shows the galvanostatic charge/discharge capacity at various C-rates (C/20, C/10, C/5 and 1C) with coulombic efficiency. Further this cell cycled up to 100 cycles. The initial charge capacity of the cell at C/20 rate is 110 mA h g^{-1} and while reversible capacity was 107 mA h g^{-1}. The good electrochemical stability of full cell demonstrates the stability of the electrode material. The specific capacity of cell is 98 mA h g^{-1} at C/10 rate. The $LiCoO_2$/LTS2 full cell also showed good rate performance, as shown in Fig. 11b. Further, work on improve the enhancement in capacity for full cell for high performance grid storage applications is in progress. In nutshell, the present versatile whatman paper template approach of synthesis will have potential to produce other active materials for battery application.

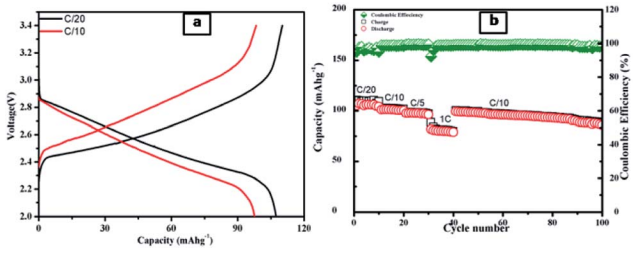

Fig. 11 (a) Galvanostatic charge–discharge voltage profiles of a $LiCoO_2$/LTS2 full cell at varied current densities within a voltage of 2–3.4 V; (b) the rate performance for $LiCoO_2$/LTS2 full cell.

5. Conclusions

Herein, we have demonstrated $Li_4Ti_5O_{12}$ and silicate modified $Li_4Ti_5O_{12}$ nanostructures using versatile paper-template technique with interconnected particle network for the first time. The present synthesis method is a new and facile technique for the modification of $Li_4Ti_5O_{12}$ which has been effectively utilized for Li ion batteries. The 2% silicate modified $Li_4Ti_5O_{12}$ anode demonstrated high ionic conductivity with lower electrochemical polarization shows enhanced electrochemical properties. The half-cell of modified LTO (LTS2) shows a high initial discharge capacity of 182 mA h g^{-1} at 50 mA g^{-1} rate between 1–2.5 V with 2% silicate compound. Significantly it shows better capacity retention when switched from higher current (1600 mA g^{-1}) to lower current (50 mA g^{-1}). It is observed that excess silicate coating on LTO lower the electrochemical performance. More significantly at optimum silicate coating on LTO shows enhanced electrochemical performance due to decrease in the charge transfer resistance by availing the Li ions. As well as ionic and electronic conductivity of LTO enhances which increases the Li ion diffusion this helps in migration and transport of electron. The present nanocomposite as an anode materials exhibit a remarkably reversible specific capacity 110 mA h g^{-1} for LIBs. More significantly, it reveals excellent rate capabilities maintained after cycling at different current densities for full cell. Therefore, it is anticipated that such a facile "versatile-template" approach with Li_2SiO_3 as a surface modifier can provide as promising platform to produce other density packed active materials for battery application (LIBs).

Conflicts of interest

There are no conflicts to declare.

Acknowledgements

Author would like to thank Ministry of Electronics and information Technology (MeitY), Government of India (No. 1(09)/2013-EMCD) and Ministry of science and technology (No. SR/WOS-A/CS-73/2017) for financial support. Authors would like to thank C-MET Pune for providing research facilities and nanocrystalline materials group for kind support.

Notes and references

1 T.-F. Yi, S.-Y. Yang and Y. Xie, *J. Mater. Chem. A*, 2015, **3**, 5750–5777.

2 T. Yuan, Z. Tan, C. Ma, J. Yang, Z. F. Ma and S. Zheng, *Adv. Energy Mater.*, 2017, **7**, 1601625.
3 X. Han, X. Gui, T.-F. Yi, Y. Li and C. Yue, *Curr. Opin. Solid State Mater. Sci.*, 2018, **22**, 109–126.
4 D. W. Murphy, R. J. Cava, S. M. Zahurak and A. Santoro, *Solid State Ionics*, 1983, **9–10**, 413–417.
5 F. Ronci, P. Reale, B. Scrosati, S. Panero, V. Rossi Albertini, P. Perfetti, M. di Michiel and J. M. Merino, *J. Phys. Chem. B*, 2002, **106**, 3082–3086.
6 K. Ariyoshi, R. Yamato and T. Ohzuku, *Electrochim. Acta*, 2005, **51**, 1125–1129.
7 T. Yuan, X. Yu, R. Cai, Y. Zhou and Z. Shao, *J. Power Sources*, 2010, **195**, 4997–5004.
8 B. Yan, M. Li, X. Li, Z. Bai, J. Yang, D. Xiong and D. Li, *J. Mater. Chem. A*, 2015, **3**, 11773–11781.
9 M. Wilkening, R. Amade, W. Iwaniak and P. Heitjans, *Phys. Chem. Chem. Phys.*, 2007, **9**, 1239–1246.
10 K. T. Fehr, M. Holzapfel, A. Laumann and E. Schmidbauer, *Solid State Ionics*, 2010, **181**, 1111–1118.
11 T. Ohzuku, A. Ueda, N. Yamamoto and Y. Iwakoshi, *J. Power Sources*, 1995, **54**, 99–102.
12 W. Wepner, P. Schmid-Beurmann and S. Scharner, *J. Electrochem. Soc.*, 1999, **146**, 857–861.
13 A. Mahmoud, J. M. Amarilla and I. Saadoune, *Electrochim. Acta*, 2015, **163**, 213–222.
14 E. Pohjalainen, T. Rauhala, M. Valkeapää, J. Kallioinen and T. Kallio, *J. Phys. Chem. C*, 2015, **119**, 2277–2283.
15 X. Bai, T. Li, Z. Dang, Y.-X. Qi, N. Lun and Y.-J. Bai, *ACS Appl. Mater. Interfaces*, 2017, **9**, 1426–1436.
16 S. Jiang, B. Zhao, Y. Chen, R. Cai and Z. Shao, *J. Power Sources*, 2013, **238**, 356–365.
17 D. Leanza, C. A. F. Vaz, I. Czekaj, P. Novak and M. El Kazzi, *J. Mater. Chem. A*, 2018, **6**, 3534–3542.
18 L. Xiaoshi, L. Ying, C. Kedi, L. Lan, Z. Qingguo and W. Hao, *Energy Technol.*, 2018, DOI: 10.1002/ente.201700982.
19 Q. Wang, S. Yang, J. Miao, M. Lu, T. Wen and J. Sun, *Appl. Surf. Sci.*, 2017, **403**, 635–644.
20 N. Sharma, D. Puthusseri, M. O. Thotiyl and S. Ogale, *ACS Omega*, 2017, **2**, 8818–8824.
21 M. Qin, Y. Li and X.-J. Lv, *Nanomaterials*, 2017, **7**(6), 150–160.
22 Y. Wang, J. Zhao, J. Qu, F. Wei, W. Song, Y.-G. Guo and B. Xu, *ACS Appl. Mater. Interfaces*, 2016, **8**, 26008–26012.
23 B. Kurc, *Ionics*, 2018, **24**, 121–131.
24 X. Li, J. Xu, P. Huang, W. Yang, Z. Wang, M. Wang, Y. Huang, Y. Zhou, M. Qu, Z. Yu and Y. Lin, *Electrochim. Acta*, 2016, **190**, 69–75.
25 H. Ge, T. Hao, H. Osgood, B. Zhang, L. Chen, L. Cui, X.-M. Song, O. Ogoke and G. Wu, *ACS Appl. Mater. Interfaces*, 2016, **8**, 9162–9169.
26 C. Zhang, D. Shao, Q. Gao, Y. Lu, Z. Liu, X. Yu, Y. Fang and D. Chen, *J. Solid State Electrochem.*, 2015, **19**, 1859–1866.
27 T.-F. Yi, Z.-K. Fang, Y. Xie, Y.-R. Zhu and S.-Y. Yang, *ACS Appl. Mater. Interfaces*, 2014, **6**, 20205–20213.
28 Z. Zhao, Y. Xu, M. Ji and H. Zhang, *Electrochim. Acta*, 2013, **109**, 645–650.
29 G. B. Xu, W. Li, L. W. Yang, X. L. Wei, J. W. Ding, J. X. Zhong and P. K. Chu, *J. Power Sources*, 2015, **276**, 247–254.
30 G. Xu, L. Yang, X. Wei, J. Ding, J. Zhong and P. K. Chu, *Adv. Funct. Mater.*, 2016, **26**, 3349–3358.
31 F. Cheng, Y. Xin, Y. Huang, J. Chen, H. Zhou and X. Zhang, *J. Power Sources*, 2013, **239**, 181–188.
32 Y. Zheng, M. Hirayama, S. Taminato, S. Lee, Y. Oshima, K. Takayanagi, K. Suzuki and R. Kanno, *J. Power Sources*, 2015, **300**, 413–418.
33 X. Yang, R. Yu, L. Ge, D. Wang, Q. Zhao, X. Wang, Y. Bai, H. Yuan and H. Shu, *J. Mater. Chem. A*, 2014, **2**, 8362–8368.
34 X. Pu and C. Yu, *Nanoscale*, 2012, **4**, 6743–6747.
35 H. Miyashiro, S. Seki, Y. Kobayashi, Y. Ohno, Y. Mita and A. Usami, *Electrochem. Commun.*, 2005, **7**, 1083–1086.
36 G. Tan, F. Wu, L. Li, R. Chen and S. Chen, *J. Phys. Chem. C*, 2013, **117**, 6013–6021.
37 H. Deng, P. Nie, H. Luo, Y. Zhang, J. Wang and X. Zhang, *J. Mater. Chem. A*, 2014, **2**, 18256–18262.
38 J. Lu, Q. Peng, W. Wang, C. Nan, L. Li and Y. Li, *J. Am. Chem. Soc.*, 2013, **135**, 1649–1652.
39 Y. Deng, J. Mou, H. Wu, N. Jiang, Q. Zheng, K. H. Lam, C. Xu and D. Lin, *Electrochim. Acta*, 2017, **235**, 19–31.
40 R. J. G. E. Ferg, A. de Kock and M. M. Thackeray, *J. Electrochem. Soc.*, 1994, **141**, 147–150.
41 T.-F. Yi, Y.-R. Zhu, W. Tao, S. Luo, Y. Xie and X.-F. Li, *J. Power Sources*, 2018, **399**, 26–41.
42 A. N. Jansen, A. J. Kahaian, K. D. Kepler, P. A. Nelson, K. Amine, D. W. Dees, D. R. Vissers and M. M. Thackeray, *J. Power Sources*, 1999, **81–82**, 902–905.
43 G. Kale, S. Arbuj, U. V. Kawade, S. Rane, J. Ambekar and B. B Kale, *Mater. Chem. Front.*, 2017, **2**, 163–170.
44 K. Kataoka, Y. Takahashi, N. Kijima, J. Akimoto and K.-i. Ohshima, *J. Phys. Chem. Solids*, 2008, **69**, 1454–1456.
45 L. Aldon, P. Kubiak, M. Womes, J. C. Jumas, J. Olivier-Fourcade, J. L. Tirado, J. I. Corredor and C. Pérez Vicente, *Chem. Mater.*, 2004, **16**, 5721–5725.
46 R. Baddour-Hadjean and J.-P. Pereira-Ramos, *Chem. Rev.*, 2010, **110**, 1278–1319.
47 T.-F. Yi, J. Shu, Y.-R. Zhu, X.-D. Zhu, C.-B. Yue, A.-N. Zhou and R.-S. Zhu, *Electrochim. Acta*, 2009, **54**, 7464–7470.
48 W. Li, M. Chen, J. Jiang, R. Wu, F. Wang, W. Liu, G. Peng and M. Qu, *J. Alloys Compd.*, 2015, **637**, 476–482.
49 J. Mosa, J. F. Vélez, J. J. Reinosa, M. Aparicio, A. Yamaguchi, K. Tadanaga and M. Tatsumisago, *J. Power Sources*, 2013, **244**, 482–487.
50 R. Lv, J. Yang, J. Wang and Y. NuLi, *J. Power Sources*, 2011, **196**, 3868–3873.
51 X. Wang, H. Hao, J. Liu, T. Huang and A. Yu, *Electrochim. Acta*, 2011, **56**, 4065–4069.
52 S. Takai, M. Kamata, S. Fujine, K. Yoneda, K. Kanda and T. Esaka, *Solid State Ionics*, 1999, **123**, 165–172.
53 L. P. An, X. P. Gao, G. R. Li, T. Y. Yan, H. Y. Zhu and P. W. Shen, *Electrochim. Acta*, 2008, **53**, 4573–4579.
54 H.-W. Lu, D. Li, K. Sun, Y.-S. Li and Z.-W. Fu, *Solid State Sci.*, 2009, **11**, 982–987.